Performance of oil sorbents based on reduced graphene oxide - silica composite aerogels

Swapneel Vijay Thakkar [a,b], Andrea Pinna[a], Carlo Maria Carbonaro [c], Luca Malfatti [d], Pablo Guardia[e], Andreu Cabot[e,f], Maria Francesca Casula[a,*]

[a]*Department of Mechanical, Chemical and Materials Engineering, CINSA and INSTM, University of Cagliari, Via Marengo 2, I-09123 Cagliari, Italy;*

[b]*Department of Chemical and Geological Sciences, University of Cagliari ,09042 Monserrato (CA), Italy*

[c]*Department of Physics, University of Cagliari ,09042 Monserrato (CA), Italy*

[8]*Department of Chemistry and Pharmacy, University of Sassari, Italy*

[e]*IREC-Catalonia Institute for Energy Research- Jardins de les Dones de Negre 1, Sant Adria de Besos, 08930 Barcelona, Spain*

[f]*ICREA, Pg. Lluis Companys 23, 08010 Barcelona, Spain*

**corresponding author: casulaf@unica.it*

Keywords: sorbent, aerogel, environmental remediation, oil spill, graphene, composite

Abstract

Clean-up of crude-oil spills ranks among the major environmental remediation issues and demands for sorbents with high and stable oleophilic and hydrophobic features. Here, aerogels with durable hydrophobicity are produced by incorporating reduced graphene oxide (rGO) in highly porous silica matrices. By a sol-gel protocol, high rGO loadings are achieved by exploiting highly dispersible hydrophilic graphene oxide as rGO precursor. Homogeneous rGO-silica composite monoliths are obtained with tunable loading up to 10 wt%, enabling a detailed analysis of the sorption behaviour towards oil spills. Composite aerogels demonstrate an excellent performance towards oil sorption with oil uptake from ~7 to ~10 times the aerogel mass. Although the sorption ability is lower than for plain hydrophobic silica, composites with a minimum loading of 5 wt% exhibit very high oil selectivity and show a durable and reliable behaviour over time, providing longer shelf-life than plain SiO_2 aerogels. The synergetic effect of rGO towards long-term hydrophobicity and oil selectivity on silica composite aerogels allows for the implementation of such composite materials in real water remediation processes.

1.1 Introduction

Over 10 million m^3 of crude oil is produced worldwide every day [1]. This oil is usually produced in remote locations and it needs to be transported to refineries for processing. In the last 5 decades, approximately 5.8 million tonnes of crude oil have been spilled into the sea during transportation [2]. These spills have a long term detrimental effect on the environment, which calls for a critical need for fast cleanup when an accident occurs [3]. Currently, the most common methods for oil spill cleanup at sea include: i) chemical methods, using dispersants/solidifiers; ii) bio-remediation, including membrane bioreactor technology; iii) *in-situ* controlled burning; iv) mechanical methods, through booms and skimmers; v) sorption [4–8]. Amongst the several strategies proposed, sorbents stand out for water spill cleanup because of the unique possibility of removal of the pollutants without effecting the environment [9,10].

The sorption capacity of a material depends on factors such as temperature, oil density, thickness of the oil film layer, as well as on intrinsic features of the sorbent material itself, such as density, porosity and oleophilic/hydrophobic properties [11–17]. There are several studies which highlight the sorption process using various kinetic models to support the experimental data describing the types of adsorption. However, a clear mechanism on the process has not been clearly understood as it involves series of steps right from point of contact to saturation [18,19]. Aerogels, being lightweight solid materials, with extremely high surface area and open porosity, are excellent candidates as sorbents [20]. In particular, owing to their huge open porosity, chemical inertness, non-toxicity, and heat resistance, silica aerogels have been widely applied to environmental cleanup and in particular to oil-spills [21–24]. The production of SiO_2 aerogels is well established and based on sol-gel technology. Wet silica gels are formed by hydrolysis and polycondensation of silica molecular precursors in alcoholic media. These gels are dried under supercritical conditions to yield highly porous

aerogels with an open mesoporous structure [25,26]. Silica aerogels produced by alcohol supercritical drying are hydrophobic in nature due to the presence of surface alkoxy groups. However, this hydrophobicity is transitory because alkoxy substituents get hydrolysed by moisture/water [27,28]. This unstable hydrophobicity is a severe drawback for practical application to spills as the sorbent activity becomes limited by a poor oil *vs.* water selectivity. In addition, the control over hydrophobicity is relevant in several other uses of silica aerogels, including thermal insulation, Cherenkov radiation detectors, drug delivery, and space applications [29–32].

Early successful strategies to produce SiO_2 aerogels with tailored hydrophobicity were based on surface modification with hydrophobic non-hydrolyzable functionalities such as fluoro-propyl. Such highly hydrophobic organosilicas have been successfully applied for water separation from organic solvents [23,24]. On the other hand, the incorporation of carbon-based nanostructures has been recently demonstrated as an excellent strategy to tune the functional properties of silica aerogels, including electrical conductivity, mechanical strength and surface area. Such C/SiO_2 composite aerogels have been used in optical and electronic devices, as thermal insulating materials and as adsorbents [33].

The production of C/SiO_2 aerogels is not straightforward: major difficulties include the tendency of the carbon nanophase to aggregate and segregate from SiO_2, as well as the limitations on precursors and solvents suitable for sol-gel chemistry. In particular, first works on graphene-SiO_2 aerogels reported very low loadings of 0.1 wt%, limited by the challenge of dispersing graphene in common solvents able to withstand supercritical drying processing [34]. Despite the very low loading, graphene-silica aerogels showed improved fire resistance, hydrophobic behaviour, and oil uptake with respect to bare silica aerogels.

Towards overcoming the low loading limitation, hydrophilic carbon nanostructures such as carbon dots and graphene oxide (GO) can be used as nanocomposite precursors owing to

their ability to disperse in common sol-gel solvents [35,36]. In particular, the production of silica aerogels filled with GO was recently addressed and shown to be a successful strategy to produce mechanically-reinforced SiO_2 monoliths [36].

In this work, the application of SiO_2 composite aerogels containing reduced graphene oxide (rGO) as oil sorbents for environmental remediation is presented. rGO is selected as an oleophilic carbon-based nanofiller which offers the advantage of higher processability under solution-based methods based on available polar precursors. Monoliths with controlled rGO loadings up to 15 wt% are produced with the use of hydrophilic GO as precursor. These undergo~~es~~ reduction during aerogel production, changing the hydrophilic nature of the composite. The obtained rGO-SiO_2 homogeneous composites are further tested as oil sorbents for environmental remediation, demonstrating their stable hydrophobicity and their high oil selectivity even in water-rich environment.

1.2 Materials and Methods

1.2.1 Materials:

Graphite flakes (~325 mesh size, 99.8% metal basis), concentrated H_2SO_4 (98%), potassium permanganate ($KMnO_4$, ACS, 99% main), sodium nitrate ($NaNO_3$, ACS,99% main) and hydrogen peroxide (H_2O_2, 35%) were purchased from Alfa Aesar. Tetraethyl orthosilicate (TEOS, $C_8H_{20}O_4Si$, reagent grade 98%), absolute ethanol (EtOH, CH_3CH_2OH, ACS reagent 99.8%), urea (CH_4N_2O, ACS reagent), mineral oil (M1180, meets USP testing specifications), and oil blue N (dye content 96%) were purchased from Sigma Aldrich.

1.2.2 Preparation of GO precursor:

GO was obtained from graphite by a modified Hummer's method [37]. Briefly, concentrated H_2SO_4 (115 mL) was added to a mixture of graphite flakes (5 g) and $NaNO_3$ (2.5 g) in a flask and was stirred at 0 ºC for 30-35 minutes. $KMnO_4$ (15 g) was gradually added in small

quantities to the mixture while keeping the reaction temperature maintained. Then, the flask was placed in a water bath at 35 ºC under stirring, until the color changed to dark brown. After which, the flask was removed from the water bath and water (230 mL) was added dropwise to the reaction mixture at room temperature under stirring. The solution was then heated at 98 ºC for 15 minutes and the reaction was stopped by removing the flask from heating mantle and rapidly adding 400 mL of water in steps and 50 mL of 35% H_2O_2 to the mixture. The mixture was allowed to settle overnight, in the following day the supernatant was decanted while the product was washed with 10% HCl solution and water until the pH of the solution became almost neutral. Finally, the solution was filtered and dried at 40 ºC, obtaining the GO powder.

1.2.3 Synthesis of rGO/silica nanocomposite aerogels:

rGO/SiO_2 nanocomposite aerogels were prepared using a one pot sol-gel method based on the co-gelation of TEOS as silica precursor and GO. The main steps involved in aerogel production are summarized in Figure SI_1, and the detailed preparation protocol is extensively described in the Supplementary Information. The sol-gel reaction was carried out under a two-step acid-base catalysis, followed by high temperature supercritical drying based on certain modifications of our previous work [38]. Briefly, TEOS was hydrolysed by an acidic hydroalcoholic solution (HNO_3 in ethanol and water). An ethanol dispersion of GO was prepared by ultrasonic treatment and added to the pre-hydrolysed TEOS under stirring. Afterwards, the mixture was subjected to basic catalysis by addition of a hydro-alcoholic solution of urea and refluxed at 85 °C. The gels were formed and aged overnight at 40 °C and then submitted to supercritical drying (up to 330 °C, 70 atm) in a Paar autoclave filled with 70 mL of absolute ethanol. The prepared aerogels will be hereafter labelled as: Si-G_x, where x is the mass loading of GO in the composite gel, and was selected as 0.1, 0.5, 1, 5, and 10

wt%. A plain silica aerogel (Si-G_0) was also prepared as a reference under the same conditions.

1.2.4 Materials Characterization.

Textural characterization was performed on a Micromeritics ASAP 2020 by determining N_2 physisorption curves at 77 K. Prior to analysis, the samples were outgassed at 200 °C for 12 hours. Surface areas were estimated using the Brunauer-Emmett-Teller (BET) model, whereas pore size and pore volumes were estimated by using the Barret–Joyner–Halenda (BJH) method.

Scanning electron microscopy (SEM) investigation was performed on a Carl ZEISS Auriga microscope with an energy dispersive X-ray spectroscopy (EDX) detector and on an ESEM FEI Quanta 200 microscope operating at 25 KV.

Finely grounded samples were characterized by transmission electron microscopy (TEM) on a Hitachi H-7000 instrument equipped with a W gun operating at 100 kV and coupled with an AMT DVC CCD camera for image acquisition.

X-ray diffraction (XRD) patterns were acquired on a Panalytical Empyrean diffractometer equipped with Cu Kα radiation, a graphite monochromator on the diffracted beam and an X'Celerator linear detector. Measurements were collected under sample spinning at 1 Hz. Fourier transform infrared (FT-IR) spectra in the Mid-IR range (4000-400 cm^{-1}) were recorded in KBr pellet on a Bruker Equinox 55 spectrometer in transmission mode.

Water contact angle (CA) measurements were carried out by means of a Kruss Drope Shape Analyzer (DSA30) and analyzed by using the Kruss Advance software through the sessile drop method. The mean CA of each measure was calculated averaging between the left and

right CA. For each sample, the measurements were repeated three times in different areas, in order to reduce errors by averaging in turn the mean CA values.

Raman spectra were acquired in backscattering geometry using 532 nm line by a wavelength stabilized diode module (LASOS DPSS series) coupled with a reflecting Bragg grating (Optigrate-Braggrade 405) to narrow the laser line. Measurements were performed at room temperature with a triple spectrometer Jobin-Yvon Dilor integrated system with a spectral resolution of about 1 cm^{-1}. Spectra were recorded in the Stokes region by a 1200 groove/mm grating monochromator and a LN-cooled charge coupled device (CCD) detector system.

1.2.5 Oil Sorption Tests

The sorption ability of the aerogels was evaluated both by mass adsorption tests and by batch adsorption assessment. Mass adsorption tests were performed at room temperature by placing a known amount of aerogel, ~30-40 mg, into a beaker containing an excess of mineral oil. The aerogel sorbents were removed after a given contact time, drained for few minutes, and weighed. It was found that all aerogels saturated after a few minutes. The aerogel oil adsorption capacity (K*o*) was determined by weighting the mass of the aerogel saturated by the adsorbed oil, based on the following formula:

$$K_o = \frac{\text{Final mass of the aerogel} - \text{Initial mass of the aerogel}}{\text{Initial mass of the aerogel}}$$

Representative digital images of the main steps in the K*o* determination are displayed in Figure SI_2 for SiO_2 and blue-dyed oil. The aerogel water sorption capacity (K*w*) was also assessed by the same approach, after the aerogel saturated by the adsorbed water.

Batch adsorption tests were also performed at room temperature (25 ºC) using oil-contaminated water at neutral pH. In these experiments the mass of aerogel was kept constant while the concentration of oil in water was varied. Briefly, 20 mg of aerogel were placed in a

250 mL beaker containing 100 mL of water with varying amounts of oil. The experiment was conducted for 50 minutes to ensure its saturation. After which, the sorbents were carefully removed and drained. The mass was measured, providing the overall liquid uptake. Then the aerogel was placed in an oven at 100 ºC overnight to remove residual water, and its mass was measured again to determine the amount of adsorbed oil.

1.3 Results and Discussion

The preparation of silica-based aerogels incorporating rGO was performed by co-gelation of the silica precursor, TEOS, and GO as described in the experimental section and depicted in Figure SI_1. Thanks to its high dispersibility in the sol-gel mixture, the GO precursor was effectively mixed in the whole compositional range investigated, giving rise to highly homogeneous sols and gels. Figure 1 shows the wet gels and the corresponding aerogels as obtained by increasing the GO loading in silica from 0 wt% to 10 wt%. The appearance of all the gels suggested a high compositional homogeneity, with no evidence of phase separation. Gel drying occurred with very limited volume shrinkage, resulting in highly homogeneous aerogels. Aerogels were extremely lightweight, with average apparent density slightly increasing with the carbon content from 0.20 to 0.21 $g \cdot cm^{-3}$. The preparation route turned out to be more effective than alternative strategies such as hydrothermal method or combined sol-gel and hydrothermal method. Those represent multistep long processes or provided poorly distributed GO or rGO, as reported in the Supplementary Information (see **Figure SI_3**).

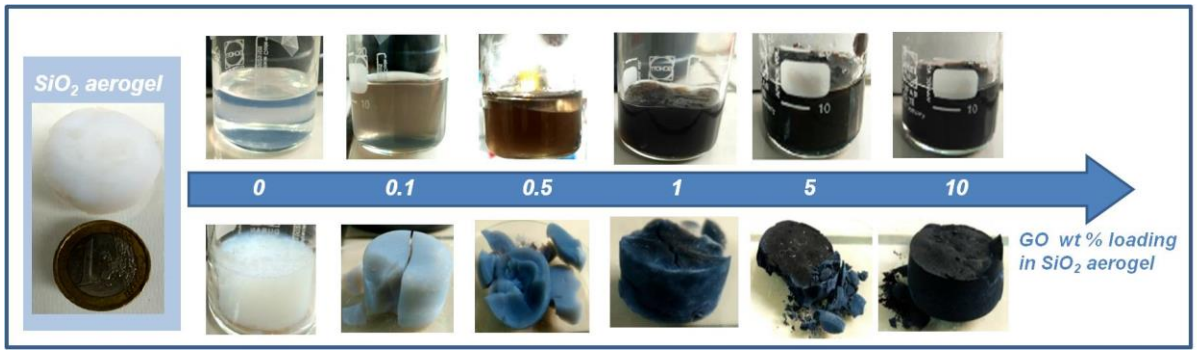

Figure 1. Visual appearance of the undoped monolithic SiO_2 aerogel (left), and of the wet gels and related aerogels obtained by increasing the loading of GO nanofiller in the silica aerogel.

The success in the formation of highly homogeneous aerogels was strongly associated with the choice of GO, with a high affinity for polar solvents required for sol-gel synthesis, as precursor of the hydrophobic rGO. While GO can be reduced to rGO upon thermal and/or chemical treatment [39], no additional step was required here to form the rGO/silica aerogel, since the initial GO precursor underwent a reduction upon supercritical drying. Indeed, the colour change accompanying the gel drying, from brown colour to greyish/black (depending on the GO loading), suggested this chemical transformation.

XRD was used to investigate the effect of processing conditions on GO. Figure 2 (A) shows the XRD patterns of the initial graphite commercial powder (G), of the GO precursor (GO), and of the thermally and chemically reduced GO (trGO and crGO, respectively). As expected, pristine graphite featured a sharp peak at 26.5° which can be ascribed to the graphitic (002) peak and is associated to atomically flat pristine graphene sheets with interlayer spacing of ~0.34 nm. The XRD pattern of the GO sample exhibited a peak at 10.6° associated to an interlayer spacing of ~0.84 nm. The increase in the distance between highly oxidised sheets reflects the presence of hydroxyls and intercalated water molecules. Chemical and thermal treatments promoted GO reduction, as suggested by the shift of peak positions to

higher diffraction angles, approaching back to its initial stage. Broadening of the peaks suggested the smaller sheet size as compared to graphite and GO, supporting effective formation of nanostructured rGO. In particular, the rGO reflections were sharper and slightly shifted to higher diffraction angles in the trGO as compared to the crGO, suggesting that thermal treatment favoured a more complete reduction and a more ordered rGO nanophase. However, XRD patterns of the aerogels did not provide conclusive evidences on the occurrence of rGO, being dominated by the scattering of amorphous silica (Figure 2B).

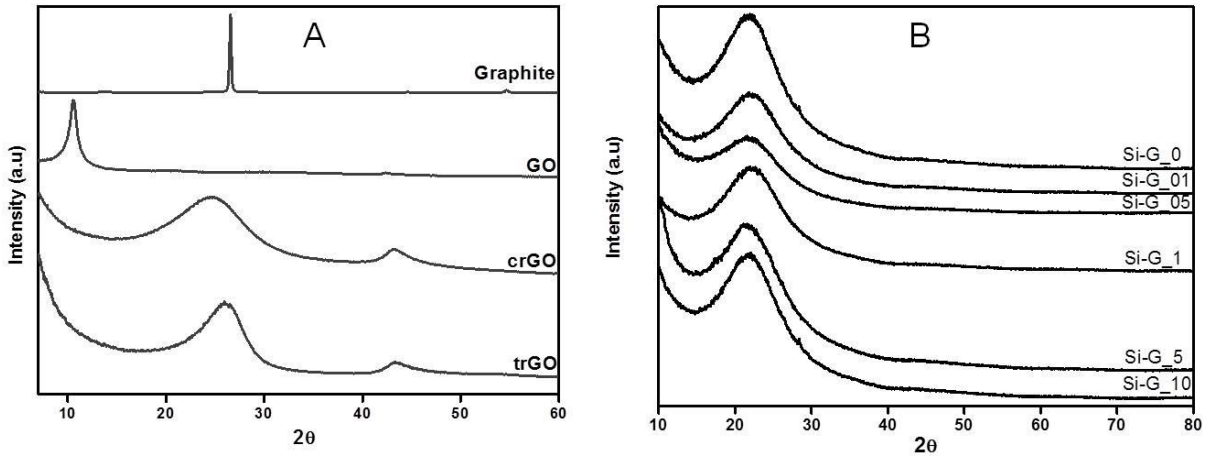

Figure 2. A) XRD pattern of graphite (G), graphene oxide (GO), chemically reduced rGO (crGO), thermally reduced rGO (trGO). B) XRD pattern of the aerogel composites with different loading of GO.

Raman spectroscopy was used to gain further insights on the produced materials, being a powerful tool to investigate the different graphene-related phases [39]. Figure 3A displays the Raman spectra of pure carbon phases as a reference. The pristine graphite sample showed the typical D, G and 2D bands at 1350 cm^{-1}, 1580 cm^{-1} and 2715 cm^{-1} respectively. These bands are associated to defect assisted one-phonon processes in disordered graphene structure (D-band), to E2g mode due to C-C stretching vibrations of sp^2 carbon systems (G-band), and to two-phonon processes at K point (2D-band) [40]. The oxidation process was accompanied by a peak shift in the Raman spectra when compared to pristine graphite, due to the disorder induced during oxidation and subsequent reduction process (based on chemical and thermal

methods), which reduced the size of the graphene sheets as already pointed out by XRD. As a control experiment, GO was submitted to the same conditions used to produce the aerogels, i.e. supercritical drying treatment under N_2 atmosphere in an autoclave up to 330 ºC in the presence of absolute ethanol. The corresponding material (SCDrGO) indeed showed a similar Raman spectrum as the chemically and thermally produced rGO.

The Raman spectra of plain SiO_2 and aerogels containing different loads of carbon fillers are displayed in Figure 3B. While no significant band was observed in the spectrum obtained from the plain SiO_2 aerogel, the D and G bands were distinctly observed at 1350 cm^{-1} and 1600 cm^{-1} in all other aerogels. The intensity of the peaks ascribed to these bands increased together with the carbon loading, as expected. As the D and G bands can be related to sp^2 and sp^3 carbon respectively, the relative intensity of these bands can be used to gain insights on the oxidation degree of graphitic phases [41]. The I_D/I_G value (see Figure SI_4) for GO was estimated 0.81, whereas for crGO was 1.08. The I_D/I_G value for the Si-G_10 aerogel was 1.01, supporting that under the conditions used to produce the aerogels, in particular during the supercritical drying step, the GO precursor was reduced, leading to nanostructured rGO dispersed within a SiO_2 aerogel matrix.

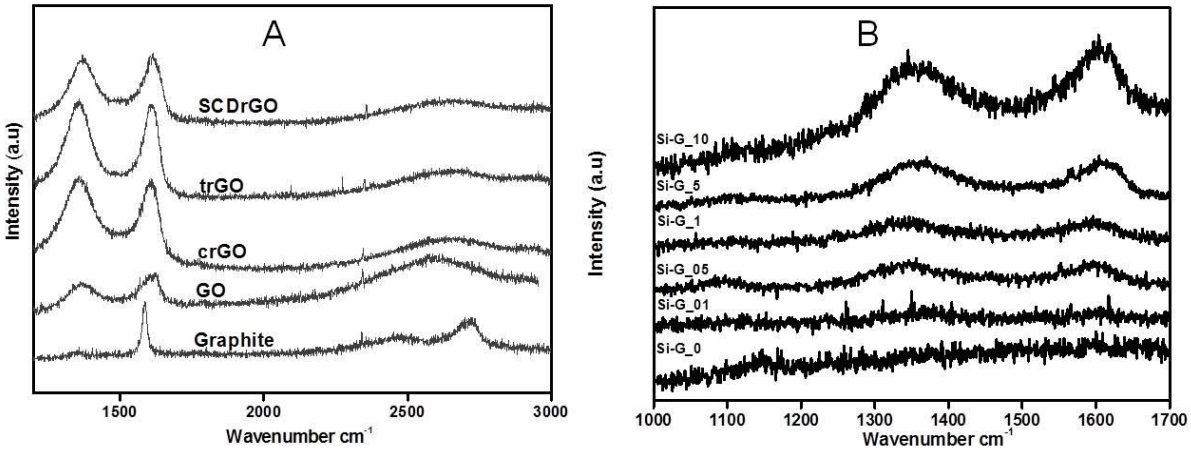

Figure 3. A) Raman spectra of pure carbon phases: pristine graphite, GO, crGO, trGO, and SCDrGO. B) Raman spectra composite aerogels containing different loads of GO, from 0 wt% up to 10 wt %.

Low magnification SEM micrographs of the composite aerogels indicated a homogeneous phase distribution at the microscale, as shown for Si-G_10 reported in Figure 4A (see also corresponding images for plain SiO_2 and for Si-G_5 in Figure SI_5). EDX microanalysis was used to provide a semiquantitative analysis of the samples and the results were in agreement with the expected composition. In particular, a carbon content of ~3 wt% was found in the plain SiO_2 aerogel, due to the occurrence of surface ethoxy groups which arise from the esterification of surface silanols during the supercritical drying process. When rGO is loaded in the aerogels, the detected C content increases to 6 % and to 11 wt % in the Si-G_5 and Si-G_10 aerogels, respectively (see Table S1). Closer inspection by high resolution SEM showed rGO nanosheets intimately blended within the silica matrix (Figure 4 B-C). rGO appears in plane view as sheets or in side view projection with the typical layered morphology. TEM investigation shows the occurrence of a highly porous silica matrix, with a non ordered and open texture typical of silica aerogels, with embedded rGO sheets (Figure 4 D-F and Figure SI_6).

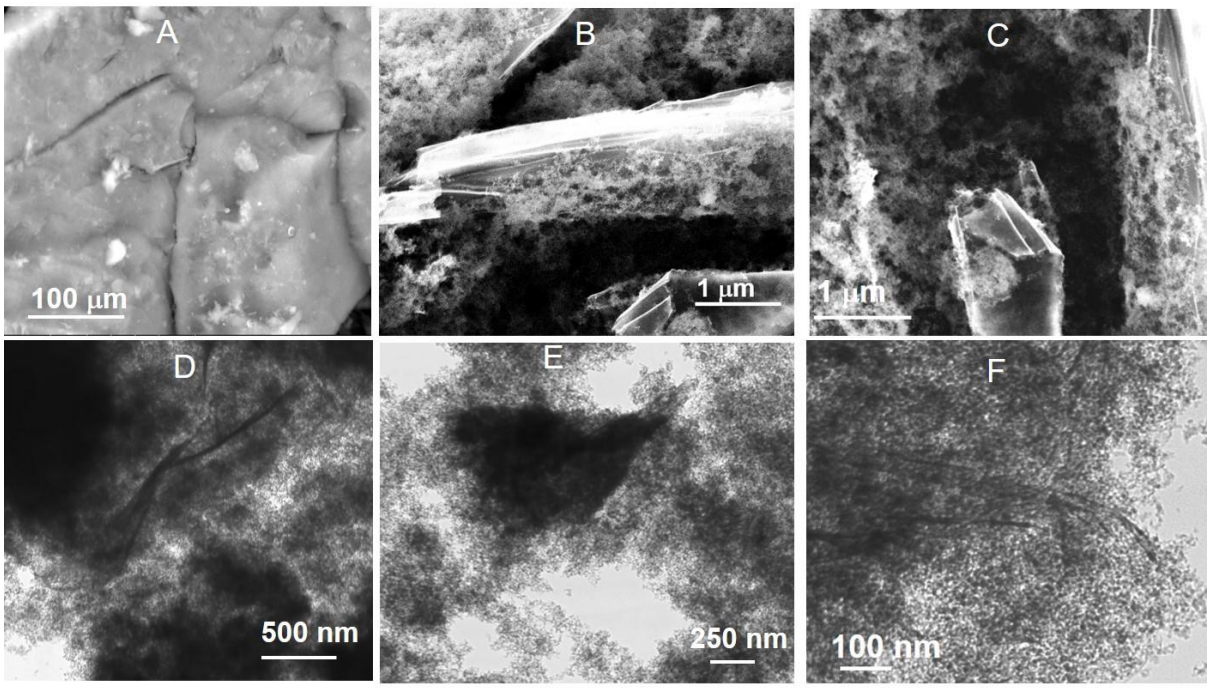

Figure 4. SEM image at low (A) and high magnification (B, C) and TEM micrographs (D-F) of Si-G_10 aerogel.

The porous texture of the aerogels was further investigated by N_2 physisorption at 77 K. Very similar isotherms, resembling those of a plain SiO_2 aerogel, were obtained for all the nanocomposite aerogels (Figure **SI_7**). This result suggested that the structure of the composites, a mesoporous structure with an average pore width of around 30 nm was mainly determined by the silica aerogel network. The main textural parameters given in Table I show that both surface areas and pore volumes were very large and they were further enhanced in the rGO-containing aerogels as compared to plain SiO_2.

Table 1. Textural parameters as obtained by N_2 physisorption measurements at 77 K for the plain SiO_2 aerogel and for the rGO-loaded aerogels.

Sample	**Surface Area ($m^2 \cdot g^{-1}$)**	**Pore volume ($cm^3 \cdot g^{-1}$)**	**Pore size (nm)**

Si-G_0	391	2.34	19
Si-G_01	588	3.42	18
Si-G_05	596	3.83	20
Si-G_1	523	3.59	21
Si-G_5	510	4.26	25
Si-G_10	522	3.67	21

For the sake of comparison, composites obtained by conventional drying (thermal treatment at 180 °C) starting from the same multicomponent gel were also prepared, obtaining so-called xerogels. As expected, the composite xerogels are relatively denser than the corresponding aerogels, as the original porous structure of the wet gel is partially collapsed during thermal drying. Figure **SI_8** shows that the xerogel with a loading of 10 wt% (X-Si-G_10 composite) is a microporous solid where the graphitic sheets are distributed on a dense silica matrix, as revealed by TEM and N_2 Physisorption. Moreover, FT-IR points out the occurrence of sol-gel hydrophilic silica typical bands.[42]

As porosity and textural features suggested that the developed aerogels might act as proper sorbents, water contact angle measurements were performed. The contact angle average value for plain SiO_2 was found to be ~106° (±3.0), indicating a hydrophobic surface. This result was expected based on the specific drying procedure used for the production of aerogels, i.e. high temperature supercritical drying from ethanol. It is well known that under these conditions, surface silanols undergo esterification by the ethoxy groups leading to hydrophobic SiO_2 [42]. Surface esterification was confirmed by the presence of vibrations corresponding to ethoxy groups in the FT-IR spectra of the plain aerogel (see Figure **SI-9**) [42]. When the silica aerogel was loaded with rGO, the average contact angle increased significantly, up to ~118° (±7), ~124° (±1), and ~131° (±1) for the aerogels loaded with 1

wt%, 5 wt%, and 10 wt % rGO, respectively (Figure 5), which denoted an increase in hydrophobicity with the rGO incorporation. This effect shows that rGO, although less effective than pure graphene, shows the expected hydrophobic features and is therefore suitable to enhance the hydrophobicity of silica aerogels.

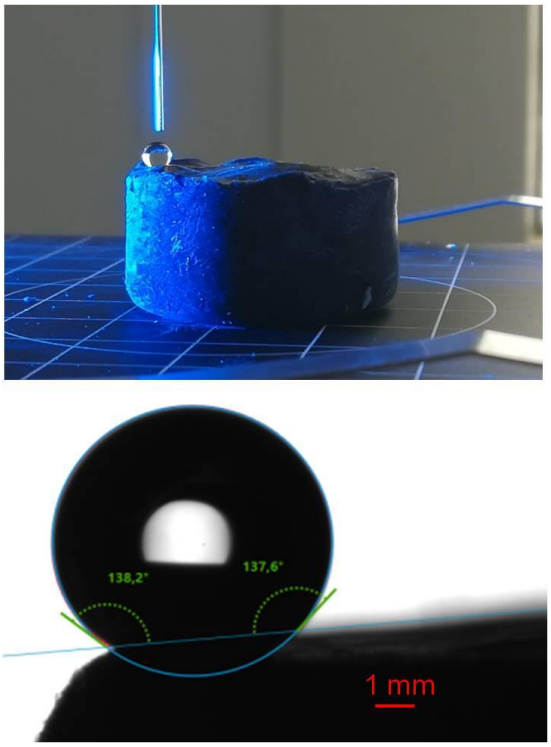

Figure 5. Digital image (top) and corresponding evaluation of the water droplet contact angle (bottom) on a Si-G_10 aerogel.

The hydrophobicity character of the aerogels was further evaluated by recording the behaviour of the aerogels released in a vial containing water over nearly 1 year. At first, all the aerogels, plain and rGO-filled, floated on water, indicating their hydrophobic nature in agreement with contact angle measurements. However, with time the plain SiO_2 aerogel changed from translucent to opaque white and partially sank in the water. On the other hand, composite aerogels kept floating on water for a much longer time. Actually, S-G_10 aerogels kept floating during all the observation period (> 6 months), as depicted in Figure SI_10~~7~~.

These data can be interpreted by taking into account that the hydrophobic nature of plain SiO_2 aerogel is due to the occurrence of a surface coverage by ethoxy groups, due to an esterification process which is well-known to take place during the supercritical drying step.[42, 43] By contact with H_2O, hydrolysis progressively takes place, and therefore over time SiO_2 aerogels become hydrophilic due to surface silanols. Conversely, the introduction of rGO nanofillers into SiO_2 aerogels results in composite materials whose hydrophobic nature is unaffected by the environmental conditions, making them more reliable than plain silica aerogels. This is of key relevance since sorbents are exposed to water during their storage and application.

To assess the potential of the developed hydrophobic aerogels as prospective oil sorbents for water remediation, sorption tests were performed. In particular, oil sorption capacity of the aerogels was determined by mass adsorption tests where a known mass of aerogel (see Fig-SI-2) was left in contact with excess oil until saturation, which occurred within 5 minutes due to the oleophilic nature of the aerogels and their fast oil uptake. The resulting oil sorption capacities of the prepared aerogels as a function of loading are reported in Table 2**.** All the aerogels acted as oil sorbents, with uptake in oil mass (K_O) decreasing upon incorporation of rGO in the silica matrix, from ~11 to ~ 7 times the mass of the aerogel itself.

Table 2. Oil sorption capacities (K_O) determined at room temperature for 5 minutes by mass adsorption tests for the fresh plain SiO_2 aerogel and rGO-loaded aerogels.

Sample	**K*o***
Si-G_0	11.10 ± 0.10
Si-G_01	9.76 ± 0.04
Si-G_05	8.39 ± 0.03
Si-G_1	8.50 ± 0.03
Si-G_5	8.05 ± 0.03
Si-G_10	7.24 ± 0.04

After being saturated with oil, the aerogels were set to flame to burn out the adsorbed oil as shown in **Figure 6** and tested again for sorption. It was found that all the tested aerogels are still able to adsorb oil, although the oil sorption ability after reuse is lower as compared to fresh aerogels and is around 5 for all the samples (see Table S2). This result could be addressed to a slightly collapse of the structure during the burning process. Besides, upon oil removal the graphitic phase could be also be affected by burning thus decreasing the sorption ability. After the second burning, the monoliths lost their mechanical stability and therefore were not suitable for further reuse.

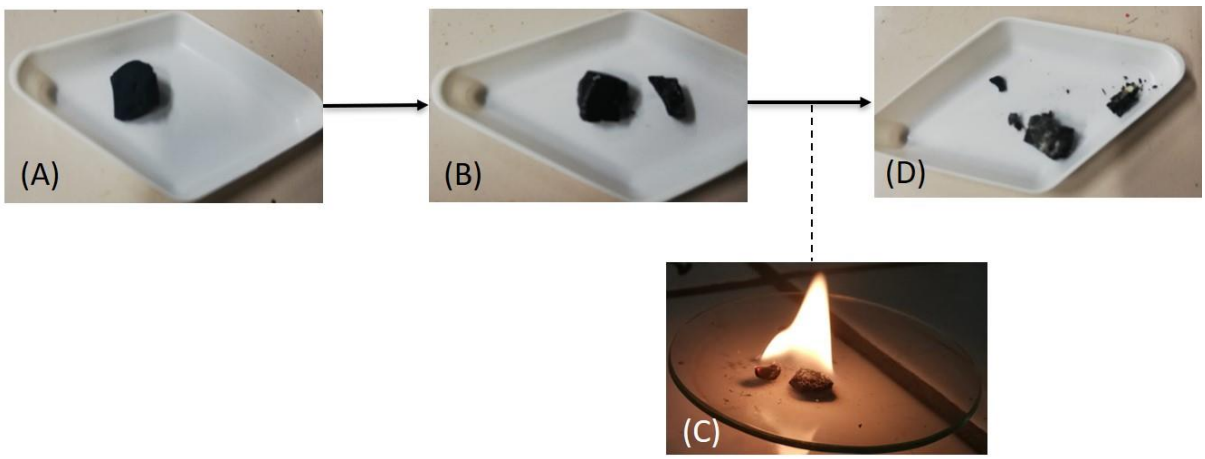

Figure 6. Digital images showing the visual appearance of a piece of Si-G_10 composite aerogel prior (A) and after oil sorption (B). The sorbent was then submitted to burning to remove the adsorbed oil (C) and submitted to reuse test (D).

A kinetic study of the sorption process was performed by removing samples after every 30 seconds to assess the sorption capacity **(Figure 7A)**. The adsorption rate is highest at the early stages (within 2 minutes) and the oil sorption capacity reaches its maximum value within 5 minutes. It is worth mentioning that after reaching saturation, *i.e.* maximum oil uptake, the aerogels upon prolonged contact with oil tend to break. This drawback somehow diverges from the mechanical reinforcement reported for silica aerogel monoliths containing GO nanofillers [36]. It should be taken into account, however, that the mechanical behaviour

of wet and swollen aerogels, although not fully elucidated, may significantly differ from that of dry aerogels [44]. The bare silica aerogel outperformed marginally the composite aerogel both in terms of speed and overall oil uptake. This might be due to the rGO sheets, which are intimately mixed with the silica matrix, which may act as oleophilic protectors for the inflow of oil into the pores also due to its wrinkled morphology. To provide further evidence that upon increasing rGO loadings the capacity was reduced, a composite sorbent with higher rGO loading (15 wt%) was prepared (see also Figure SI_11 for visual appearance and TEM images). As expected, it was found that the sorption ability further decreased 6.57 $\pm$ 0.05. To get a more comprehensive picture of the sorption behaviour of the aerogels, the water sorption capacity K*w* over time was measured (**Figure 7B**). Although water sorption was very rapid, reaching saturation within few minutes, the test was also carried out for a long duration to get precise values. It is worth mentioning that the aerogels did not break during this test. Interestingly, the silica aerogel- being exposed to moisture and water-rich environment- tends to uptake water and indeed showed a water sorption ability as assessed by the adsorption capacity value (K_w) higher than for oil (K_o). The sorption ability of silica aerogels has been previously shown to depend on the features of the liquid, such as polarity, surface tension and molecular structure.[43] In particular, water molecules may interact also through hydrogen bonding with surface silanols. Aerogels containing rGO fillers adsorbed much less H_2O as compared to plain silica, and composite aerogels with high rGO loading (5 wt%, 10 wt %, and 15 wt %) adsorbed no water at all.

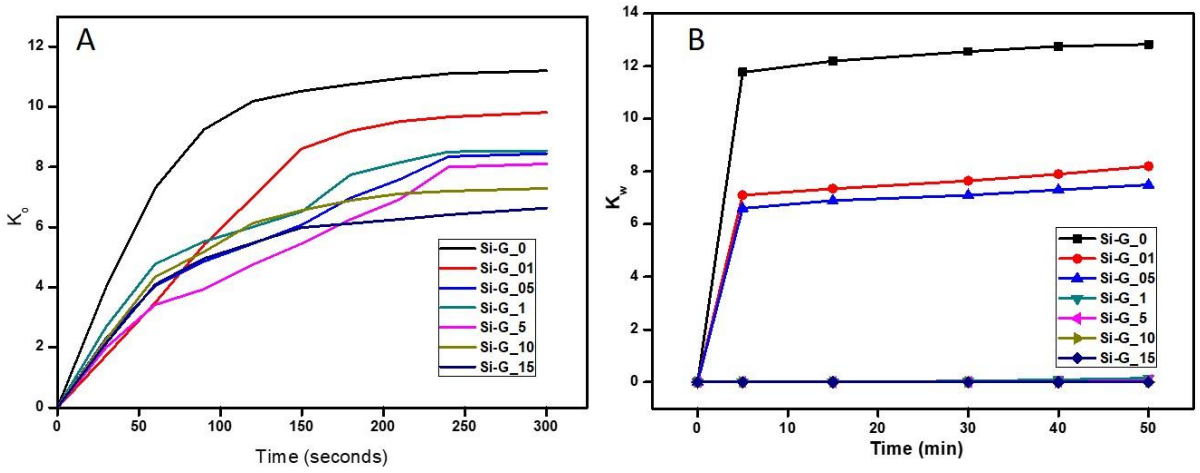

Figure 7. Kinetics of oil (A) and water (B) mass sorption as evaluated by the corresponding sorption capacity K_o and K_w, respectively, for the plain SiO_2 aerogel and for the rGO-loaded aerogels.

Overall, it can be deduced that 5 wt% is the optimal rGO loading into silica aerogels to produce effective oleophilic sorbents for water remediation, as for this composition high and selective oil sorption ability (eight times the sorbent mass) is recorded together with durable hydrophobicity. Batch adsorption tests were additionally performed, where the oil and water sorption from the aerogel was assessed in an oil-water mixture at room temperature. In this case, the mass of the aerogel was kept constant while varying the oil concentration, and the adsorbed mass was evaluated after 50 minutes. The outcome of these experiments is summarized in **Figure 8**. The rGO-filled aerogels adsorbed increasing amounts of oil while adsorbing very limited amount of water. In contrast to adsorption tests in pure water, a slight water uptake was measured in water-oil combinations for the composite aerogels, due to the interfacial interaction between oil and water. Indeed, the hydrophilic and hydrophobic properties of graphitic phases have been revisited with particular reference to their behaviour in water-oil mixtures, and their amphiphilic behaviour as well as their ability to act as surfactant has been demonstrated [45–47].

The water adsorption was in any case very limited (0.01-0.03 g). All aerogels had a similar trend up to 150 mg of oil where nearly all the oil in the mixture was effectively adsorbed by the aerogel. When a large excess of oil was added as compared to the sorbent mass, (i.e. around a 10-fold excess of oil in mass) the apparent decrease in oil sorption is actually due to loss of mechanical stability of the aerogels, resulting in a large error in oil uptake assessment. As an alternative approach, oil sorbents based on silica nanoparticles introduced into GO sponges have been recently reported [48]. Remarkably, organic solvents sorption capacities in the same range were obtained (~8-10), and an active role of silica nanoparticles in preventing deformation of the GO sponge and breakage was found.

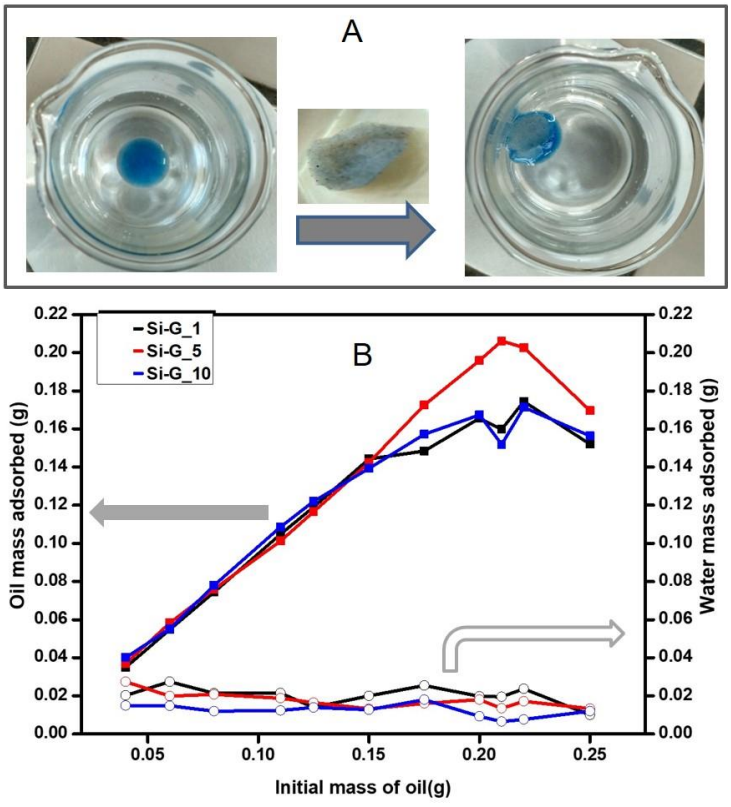

Figure 8. rGO-SiO_2 nanocomposite aerogel (Si-G_1) sorbent for batch sorption tests on oil-water mixture; (A) Oil mass uptake ~~(M_O)~~ and water mass uptake ~~(M_W)~~ from the rGO-SiO_2 aerogels with loading content 1 wt%, 5 wt%, 10 wt% as assessed by batch adsorption tests (B). Full square symbols and empty circle symbols refer to oil mass and to water mass adsorption, respectively.

1.4 Conclusions

The prospective application of composite aerogels made out of rGO nanofillers loaded within highly porous SiO_2 as novel sorbents for oil spills has been investigated. TEM, SEM and N_2 porosimetry indicate that the rGO nanostructures were homogeneously distributed within the SiO_2 porous texture and that the two phases were intimately blended in the whole investigated composition range (loading from 0 to 15 wt%). Effective loading of the rGO nanofillers within the aerogel was achieved by exploiting a precursor, which can be easily incorporated within silica sol-gel chemistry such as GO. Raman spectroscopy and water contact angle measurements support that the conditions used for aerogel production by high temperature supercritical drying of the solvent favour reduction of the parent GO phase, resulting in the production of rGO-SiO_2 composite aerogels.

Oil sorption experiments showed that composite aerogels were highly active oil sorbents, with sorption capacity values of ~7 - 11 times the mass of the sorbent and decreasing with the amount of rGO. rGO-SiO_2 composite aerogels showed a much higher selectivity towards oil rather than water as compared to plain SiO_2, making these sorbents more effective for application in environmental remediation. In addition, while the hydrophobic features of plain SiO_2 aerogels were progressively lost in water/moisture rich environment due to surface hydrolysis processes, rGO-SiO_2 composite aerogels showed durable hydrophobicity. The proposed study demonstrated the potential of C-based nanostructures as a means to produce hydrophobic silica-based oil sorbents with improved oil selectivity and more durable shelf life.

1.5 Acknowledgements

Dr. Danilo Loche is kindly acknowledged for helpful discussion. We acknowledge the CeSAR (Centro Servizi d'Ateneo per la Ricerca) of the University of Cagliari, Italy for the scanning electron microscopy experiments performed with ESEM FEI Quanta 200 microscope and Dr. Marco Marceddu for technical support. MFC and AC thank University of Cagliari and Regione Autonoma della Sardegna for funding under MGR project "Composite Materials for Water Remediation" CUP: F21I17000040002.

1.6 Declaration of interests: none

1.7 Supplemental Information: Detailed description of aerogel production and synthesis schematic; Features of composites obtained by alternative synthetic routes; Schematic of the oil sorption experiments; Detail on Raman spectra analysis; Additional SEM and TEM micrographs and related microanalysis results; N_2 physisorption isotherms and BJH pore size distribution plots; FT-IR spectra; Sorbent floating tests, TEM and visual appearance of aerogels with 15 wt% loading, reusability test results.

1.8 References

[1] U.S. Energy Information Administration (EIA), Short-Term Energy Outlook (STEO) Forecast highlights, 2020. https://www.eia.gov/outlooks/steo/pdf/steo_full.pdf.

[2] The International Tanker Owners Pollution Federation Limited, OIL TANKER SPILL STATISTICS 2017, 2018. https://www.itopf.org/fileadmin/data/Photos/Statistics/Oil_Spill_Stats_2017_web.pdf.

[3] The International Tanker Owners Pollution Federation Limited, Effects of Oil Pollution on the Marine Environment, Tech. Inf. Pap. 13 (2013) 4. https://www.itopf.org/knowledge-

resources/documents-guides/document/tip-13-effects-of-oil-pollution-on-the-marine-environment/.

[4] I.B. Ivshina, M.S. Kuyukina, A. V. Krivoruchko, A.A. Elkin, S.O. Makarov, C.J. Cunningham, T.A. Peshkur, R.M. Atlas, J.C. Philp, Oil spill problems and sustainable response strategies through new technologies, Environ. Sci. Process. Impacts. 17 (2015) 1201–1219. doi:10.1039/C5EM00070J.

[5] M. Fingas, The basics of Oil spill cleanup, Third Edit, CRC press, 2012.

[6] A. Sepehri, M. Sarrafzadeh, Effect of nitrifiers community on fouling mitigation and nitrification efficiency in a membrane bioreactor, Chem. Eng. Process. Process Intensif. 128 (2018) 10–18. doi:10.1016/j.cep.2018.04.006.

[7] A. Sepehri, M.H. Sarrafzadeh, Activity enhancement of ammonia - oxidizing bacteria and nitrite - oxidizing bacteria in activated sludge process : metabolite reduction and - CO2 mitigation intensification process, Appl. Water Sci. 9 (2019) 1–12. doi:10.1007/s13201-019-1017-6.

[8] G. Mannina, A. Cosenza, D. Di Trapani, M. Capodici, G. Viviani, Membrane bioreactors for treatment of saline wastewater contaminated by hydrocarbons (diesel fuel): An experimental pilot plant case study, Chem. Eng. J. 291 (2016) 269–278. doi:10.1016/j.cej.2016.01.107.

[9] X. Gao, Y. Zhou, S. Liu, Y. Tan, Z. Cheng, Z. Shen, FeN3 -embedded carbon as an efficient sorbent for mercury adsorption : A theoretical study, 374 (2019) 1337–1343. doi:10.1016/j.cej.2019.04.189.

[10] W. Wang, Z. Xu, X. Zhang, A. Wimmer, E. Shi, Y. Qin, X. Zhao, B. Zhou, L. Li, Rapid and efficient removal of organic micropollutants from environmental water using a magnetic nanoparticles-attached fluorographene-based sorbent, Chem. Eng. J. 343 (2018) 61–68. doi:10.1016/j.cej.2018.02.101.

[11] D.A. Baiseitov, M.I. Tulepov, L.R. Sassykova, S.E. Gabdrashova, G.A. Essen, K.K. Kudaibergenov, Z.A. Mansurov, Sorption capacity of the oil sorbents for the removal of thin films of oil, Bulg. Chem. Commun. 49 (2017) 335–338.

[12] O.O. Sulaiman, W.B. Wan Nik, A.H. Saharuddin, A.S.A. Kader, Study of packing density and temperature on the oil sorption capacity of packed local kapok fiber as bio-oil spill absorbent, Biosci. Biotechnol. Res. Asia. 9 (2012) 53–61. doi:10.13005/bbra/966.

[13] M. Inagaki, F. Kang, M. Toyoda, H. Konno, Carbon Materials for Spilled-oil Recovery, in: M. Inagaki, F. Kang, M. Toyoda, H. Konno (Eds.), Adv. Mater. Sci. Eng. Carbon, Elsevier Inc., 2014: pp. 313–334. doi:10.1016/B978-0-12-407789-8.00014-4.

[14] S. Gupta, N.H. Tai, Carbon materials as oil sorbents: A review on the synthesis and performance, J. Mater. Chem. A. 4 (2016) 1550–1565. doi:10.1039/c5ta08321d.

[15] J. Ge, H.Y. Zhao, H.W. Zhu, J. Huang, L.A. Shi, S.H. Yu, Advanced Sorbents for Oil-Spill Cleanup: Recent Advances and Future Perspectives, Adv. Mater. 28 (2016) 10459–10490. doi:10.1002/adma.201601812.

[16] O.S.H. Santos, M.C. Silva, M.I. Yoshida, Synthesis and performance of different polyurethane foams as oil sorbents, J. Appl. Polym. Sci. 134 (2017) 45409 (1–8). doi:10.1002/app.45409.

[17] M.I. Al-biloushi, H. Milliman, M.D. Gawryla, D.A. Schiraldi, Oil absorption performance of polymer / clay aerogel materials, J. Appl. Polym. Sci. 135 (2018) 45844 (1–10). doi:10.1002/app.45844.

[18] H. Choi, J.P. Moreau, Oil Sorption Behavior of Various Sorbents Studied by Sorption Capacity Measurement and Environmental Scanning Electron Microscopy, Microsc. Res. Tech. 25 (1993) 447–455. doi:10.1002/jemt.1070250516.

[19] Y.S. Ho, J.C.Y. Ng, G. McKay, Kinetics of pollutant sorption by biosorbents: Review, Sep. Purif. Methods. 29 (2000) 189–232. doi:10.1081/SPM-100100009.

[20] H. Maleki, Recent advances in aerogels for environmental remediation applications: A review, Chem. Eng. J. 300 (2016) 98–118. doi:10.1016/j.cej.2016.04.098.

[21] M.L.N. Perdigoto, R.C. Martins, N. Rocha, M.J. Quina, L. Gando-Ferreira, R. Patrício, L. Durães, Application of hydrophobic silica based aerogels and xerogels for removal of toxic organic compounds from aqueous solutions, J. Colloid Interface Sci. 380 (2012) 134–140. doi:10.1016/j.jcis.2012.04.062.

[22] S. Štandeker, Z. Novak, Ž. Knez, Adsorption of toxic organic compounds from water with hydrophobic silica aerogels, J. Colloid Interface Sci. 310 (2007) 362–368. doi:10.1016/j.jcis.2007.02.021.

[23] J.G. Reynolds, P.R. Coronado, L.W. Hrubesh, Hydrophobic aerogels for oil-spill cleanup - Intrinsic absorbing properties, Energy Sources. 23 (2001) 831–843. doi:10.1080/009083101316931906.

[24] L.W. Hrubesh, P.R. Coronado, J.H. Satcher, Solvent removal from water with hydrophobic aerogels, J. Non. Cryst. Solids. 285 (2001) 328–332. doi:10.1016/S0022-3093(01)00475-6.

[25] T.M. Tillotson, L.W. Hrubesh, Transparent ultralow-density silica aerogels prepared by a two-step sol-gel process, J. Non. Cryst. Solids. 145 (1992) 44–50. doi:10.1016/S0022-3093(05)80427-2.

[26] A. Corrias, M.F. Casula, Aerogels Containing Metal, Alloy, and Oxide Nanoparticles Embedded into Dielectric Matrices, in: M.M. Koebel, Michel A. Aegerter, Nicholas Leventis (Ed.), Aerogels Handb., Springer US, 2011: pp. 335–363. doi:10.1007/978-1-4419-7589-8.

[27] M.O. Adebajo, R.L. Frost, J.T. Kloprogge, O. Carmody, S. Kokot, Porous Materials for Oil Spill Cleanup : A Review of Synthesis and Absorbing Properties, J. Porous Mater. 10 (2003) 159–170. doi:10.1023/A:1027484117065.

[28] A.S. Dorcheh, M.H. Abbasi, Silica aerogel synthesis , properties and characterization, J.

Mater. Process. Technol. 199 (2008) 10–26. doi:10.1016/j.jmatprotec.2007.10.060.

[29] G. Hayase, K. Kanamori, K. Abe, H. Yano, A. Maeno, H. Kaji, Polymethylsilsesquioxane − Cellulose Nanofiber Biocomposite Aerogels with High Thermal Insulation , Bendability , and Superhydrophobicity, Appl. Mater. Interfaces. 6 (2014) 9466–9471. doi:10.1021/am501822y.

[30] A.K. Gougas, D. Ilie, S. Ilie, V. Pojidaev, Behavior of hydrophobic aerogel used as a Cherenkov medium, Nucl. Instruments Methods Phys. Res. Sect. A Accel. Spectrometers, Detect. Assoc. Equip. 421 (1999) 249–255. doi:10.1016/S0168-9002(98)01192-9.

[31] L.W. Hrubesh, Aerogel applications, J. Non. Cryst. Solids. 225 (1998) 335–342. doi:http://dx.doi.org/10.1016/S0022-3093(98)00135-5.

[32] I. Smirnova, J. Mamic, W. Arlt, Adsorption of drugs on silica aerogels, Langmuir. 19 (2003) 8521–8525. doi:10.1021/la0345587.

[33] A. Lamy-Mendes, R.F. Silva, L. Durães, Advances in carbon nanostructure-silica aerogel composites: A review, J. Mater. Chem. A. 6 (2018) 1340–1369. doi:10.1039/c7ta08959g.

[34] D. Loche, L. Malfatti, D. Carboni, V. Alzari, A. Mariani, M.F. Casula, Incorporation of graphene into silica-based aerogels and application for water remediation, RSC Adv. 6 (2016) 66516–66523. doi:10.1039/c6ra09618b.

[35] K. Suzuki, L. Malfatti, D. Carboni, D. Loche, M. Casula, A. Moretto, M. Maggini, M. Takahashi, P. Innocenzi, Energy Transfer Induced by Carbon Quantum Dots in Porous Zinc Oxide Nanocomposite Films, J. Phys. Chem. C. 119 (2015) 2837–2843. doi:10.1021/jp510661d.

[36] Y. Lei, Z. Hu, B. Cao, X. Chen, H. Song, Enhancements of thermal insulation and mechanical property of silica aerogel monoliths by mixing graphene oxide, Mater. Chem. Phys. 187 (2017) 183–190. doi:10.1016/j.matchemphys.2016.11.064.

[37] L. Company, B. William, R.E. Offeman, Preparation of Graphitic Oxide, J. Am. Chem. Soc.

80 (1958) 1339. doi:10.1021/ja01539a017.

[38] M.F. Casula, D. Loche, S. Marras, G. Paschina, A. Corrias, Role of Urea in the Preparation of Highly Porous Nanocomposite Aerogels, Langmuir. 23 (2007) 3509–3512. doi:10.1021/la0635799.

[39] W. Gao, L.B. Alemany, L. Ci, P.M. Ajayan, New insights into the structure and reduction of graphite oxide, Nat. Chem. 1 (2009) 403–408. doi:10.1038/nchem.281.

[40] L.M. Malard, M.A. Pimenta, G. Dresselhaus, M.S. Dresselhaus, Raman spectroscopy in graphene, Phys. Rep. 473 (2009) 51–87. doi:10.1016/j.physrep.2009.02.003.

[41] C.M. Carbonaro, R. Corpino, M. Salis, F. Mocci, S.V. Thakkar, C. Olla, P.C. Ricci, On the Emission Properties of Carbon Dots : Reviewing Data and Discussing Models, C-Journal Carbon Res. 5 (2019) 1–15. doi:10.3390/c5040060.

[42] M. Casu, M.F. Casula, A. Corrias, G. Paschina, Textural characterization of high temperature silica aerogels, J. Non. Cryst. Solids. 315 (2003) 97–106. doi:10.1016/S0022-3093(02)01596-X.

[43] A.M. Anderson, M.K. Carroll, Hydrophobic Silica Aerogels: Review of Synthesis, Properties and Applications, in: Michel A. AegerterNicholas LeventisMatthias M. Koebel (Ed.), Aerogels Handb., Springer US, 2011: pp. 47–77. doi:10.1007/978-1-4419-7589-8.

[44] S. Antonyuk, S. Heinrich, P. Gurikov, S. Raman, I. Smirnova, Influence of coating and wetting on the mechanical behaviour of highly porous cylindrical aerogel particles, Powder Technol. 285 (2015) 34–43. doi:10.1016/j.powtec.2015.05.004.

[45] J. Kim, L.J. Cote, F. Kim, W. Yuan, K.R. Shull, J. Huang, Graphene Oxide Sheets at Interfaces, J. Am. Chem. Soc. 132 (2010) 8180–8186. doi:10.1021/ja102777p.

[46] T.M. Mccoy, M.J. Pottage, R.F. Tabor, Graphene Oxide-Stabilized Oil-in-Water Emulsions: pH-Controlled Dispersion and Flocculation, J. Phys. Chem. C. 118 (2014) 4529–4535.

doi:10.1021/jp500072a.

[47] T.D. Gamot, A.R. Bhattacharyya, T. Sridhar, F. Beach, R.F. Tabor, M. Majumder, Synthesis and Stability of Water-in-Oil Emulsion Using Partially Reduced Graphene Oxide as a Tailored Surfactant, Langmuir. 33 (2017) 10311–10321. doi:10.1021/acs.langmuir.7b02320.

[48] X. Zhao, Y. Zhu, Y. Wang, Z. Li, Y. Sun, S. Zhao, X. Wu, D. Cao, Hydrophobic , blocky silica-reduced graphene oxide hybrid sponges as highly efficient and recyclable sorbents, Appl. Surf. Sci. 486 (2019) 303–311. doi:10.1016/j.apsusc.2019.05.017.